



Contents lists available at ScienceDirect

Biochemical and Biophysical Research Communications

journal homepage: www.elsevier.com/locate/ybbrc

Crystal structure of substrate-bound bifunctional proline racemase/hydroxyproline epimerase from a hyperthermophilic archaeon

Yasunori Watanabe ^{a, b}, Seiya Watanabe ^{a, b, c, *}, Yoshika Itoh ^b, Yasuo Watanabe ^{a, b}

^a Department of Bioscience, Graduate School of Agriculture, Ehime University, 3-5-7 Tarumi, Matsuyama, Ehime, 790-8566, Japan

^b Faculty of Agriculture, Ehime University, 3-5-7 Tarumi, Matsuyama, Ehime, 790-8566, Japan

^c Center for Marine Environmental Studies (CMES), Ehime University, 2-5 Bunkyo-cho, Matsuyama, Ehime, 790-8577, Japan

ARTICLE INFO

Article history:

Received 23 January 2019

Accepted 31 January 2019

Available online xxx

Keywords:

Proline racemase

Hydroxyproline 2-epimerase

Hyperthermophilic archaeon

Thermococcus litoralis

Crystal structure

ABSTRACT

The hypothetical OCC_00372 protein from *Thermococcus litoralis* is a member of the ProR superfamily from hyperthermophilic archaea and exhibits unique bifunctional proline racemase/hydroxyproline 2-epimerase activity. However, the molecular mechanism of the broad substrate specificity and extreme thermostability of this enzyme (TlProR) remains unclear. Here we determined the crystal structure of TlProR at 2.7 Å resolution. Of note, a substrate proline molecule, derived from expression host *Escherichia coli* cells, was tightly bound in the active site of TlProR. The substrate bound structure and mutational analyses suggested that Trp241 is involved in hydroxyproline recognition by making a hydrogen bond between the indole group of Trp241 and the hydroxyl group of hydroxyproline. Additionally, Tyr171 may contribute to the thermostability by making hydrogen bonds between the hydroxyl group of Tyr171 and catalytic residues. Our structural and functional analyses provide a structural basis for understanding the molecular mechanism of substrate specificity and thermostability of ProR superfamily proteins.

© 2019 Elsevier Inc. All rights reserved.

1. Introduction

Proline racemase (EC 5.1.1.4; ProR) is a member of the pyridoxal 5'-phosphate-independent racemase family (COG3938), and catalyzes the deprotonation/reprotonation of the chiral carbon (C α) of proline, resulting in the stereo inversion of chiral centers [1–3]. Its catalysis is based on the same 1,1-proton transfer mechanism using two general acidic/basic cysteine residues located on opposite faces of the active site. In specific clostridium bacteria [4,5] and *Trypanosoma* species [6–10], ProR is involved in the utilization of L-proline with the production of 5-aminopentanoate (so-called “Stickland fermentation”), and the mechanisms underlying the escape of parasites from host immunity as a B-cell mitogen, respectively.

L-Hydroxyproline (L-Hyp) has been found in specific proteins including collagen, the cell wall of plants, and some peptide antibiotics. In mammalian and plant systems, L-proline residues are post-translationally hydroxylated to *trans*-4-hydroxy-L-proline (T4LHyp) and/or *trans*-3-hydroxy-L-proline (T3LHyp) [11].

Alternatively, direct biosynthesis from free L-proline to L-Hyp, including T4LHyp and T3LHyp, has been identified in a few bacteria and fungi that produce peptide antibiotics [12]. The catabolism of L-Hyp by (micro)organisms has recently been investigated at the molecular level. Among them, hydroxyproline 2-epimerase (EC 5.1.1.8; HypE) is responsible for the first step of the T4LHyp metabolic pathway from bacteria and catalyzes the isomerization of T4LHyp to *cis*-4-hydroxy-D-proline (C4DHyp), with the final product being α -ketoglutarate [13,14]. On the other hand, in mammals, bacteria, and archaea, T3LHyp is converted to Δ^1 -pyrroline-2-carboxylate by T3LHyp dehydratase (EC 4.2.1.77; T3LHypD), with the final product being L-proline [15–17]. HypE and T3LHypD belong to the COG3938 protein superfamily, and the former possesses two equivalent cysteine residues with ProR at the active sites, conforming to their homologous reactions [15,18]. On the other hand, the substrate specificities of ProR and HypE are very strict.

Although the ProR-like protein was only originally considered to be present in mesophilic eukaryotes, bacteria, and fungi, we recently showed that the hypothetical OCC_00372 and OCC_00387 proteins from the hyperthermophilic archaea *Thermococcus litoralis* functioned as ProR (TlProR) and T3LHypD, respectively [17,19]. The former is of interest because not only L-proline, but also T4LHyp and T3LHyp are significant substrates; to the best of our knowledge, this

* Corresponding author. Department of Bioscience, Graduate School of Agriculture, Ehime University, 3-5-7 Tarumi, Matsuyama, Ehime, 790-8566, Japan.

E-mail address: irab@agr.ehime-u.ac.jp (S. Watanabe).

is the first example of a bifunctional ProR/HypE. Although a site-directed mutagenic analysis revealed several important amino acid residues for the recognition of hydroxyproline (more hydrophilic and bulkier than proline), it was unsuccessful for completely eliminating HypE activity similar to a natural ProR enzyme [19]. To gain mechanistic insights into the unique substrate specificity and extreme thermostability, we determined the crystal structure of TlProR. Intriguingly, a proline molecule derived from *E. coli* cells was tightly bound in the active site of TlProR during purification and crystallization. Structure-based mutational analyses showed that Trp241 in the substrate binding site is responsible for substrate specificity for hydroxyproline and that Tyr171 might contribute to the thermostability by making hydrogen bonds to the side chains of catalytic residues. The crystal structure of TlProR bound with proline gives a basis for understanding the molecular mechanism of substrate specificity and thermostability.

2. Materials and methods

2.1. Protein expression and purification

The TlProR gene from *T. litoralis* DSM5473 (OCC_00372) was previously cloned into pETDuet-1 (Novagen), a plasmid vector that encodes the addition of an N-terminal (His)₆ tag on the proteins expressed [19]. Mutations for the described amino-acid substitutions were introduced by PCR-based site-directed mutagenesis. To construct *E. coli* expression plasmids for L-proline dehydrogenase (L-ProDH) from *Aeropyrum pernix* [20,21], the gene encoding the enzyme (APE_1267.1) was amplified by PCR from the *A. pernix* genome, digested using *Bam*HI and *Kpn*I, and cloned into pETDuet-1 using the same sites. To construct *E. coli* expression plasmids for D-proline dehydrogenase (D-ProDH) from *Pyrobaculum islandicum* [22], the synthetic gene optimized with *E. coli* codon usage was obtained from Eurofins Genomics, digested using *Bam*HI and *Xho*I, and cloned into pETDuet-1 using the same sites. All of the constructs were sequenced to confirm their identities. Target proteins with 14 additional residues (MGSSHHHHHSQDL) at their N-terminus, were expressed in *E. coli* strain BL21-CodonPlus(DE3)-RIL cells (Novagen) cultured in Luria-Bertani (LB) medium containing ampicillin (100 mg L⁻¹) and chloramphenicol (30 mg L⁻¹) at 37 °C. When the optical density of the culture at 600 nm reached ~0.8, isopropyl-β-D-thiogalactopyranoside (IPTG) was added to a final concentration of 0.1 mM to induce protein expression. After the addition of IPTG, the cultures were grown at 20 °C for a further 20 h in order to induce the expression of the target proteins. The cells were harvested, resuspended in Buffer A (50 mM sodium phosphate pH 8.0, 500 mM NaCl, and 20 mM imidazole), disrupted by sonication, and then centrifuged to pellet the insoluble debris. The supernatant was loaded onto a Ni-NTA Superflow column (Qiagen) equilibrated with lysis buffer. After washing the column with Buffer A, target proteins were eluted using Buffer B (50 mM sodium phosphate pH 8.0, 100 mM NaCl, and 250 mM imidazole). Expression and purification of C4DHyp dehydrogenase (D-HypDH) was carried out as described previously [23]. L-ProDH, D-ProDH, and D-HypDH were then dialyzed against Buffer C (20 mM Tris-HCl pH 8.0 containing 150 mM NaCl). TlProR was further purified by size-exclusion chromatography using a HiLoad 16/600 Superdex 200-pg column (GE Healthcare) eluted with Buffer C. The main single-peak fractions were collected and concentrated by ultrafiltration with Amicon Ultra-15 (Millipore).

2.2. Crystallization and X-ray crystallography

Crystallization screening was performed at 20 °C using the sitting-drop vapor-diffusion method. Each drop was formed by

mixing equal volumes (0.5 μL) of protein solution (23 mg mL⁻¹ TlProR in Buffer C) and reservoir solution, and equilibrated against 70 μL of reservoir solution. TlProR crystals were obtained using reservoir solution consisting of 0.1 M HEPES pH 7.0 and 30% (v/v) Jeffamine ED-2001 pH 7.0. Because the concentration of Jeffamine ED-2001 in the reservoir solution was sufficient as a cryoprotectant, the crystal of TlProR was directly mounted on a nylon loop and then flash-cooled and maintained in a stream of nitrogen gas at 100 K during data collection. X-ray diffraction data were collected on a MAR225HE charge-coupled device detector using beamline BL38B1, SPring-8 (Hyogo, Japan) at a wavelength of 1.00 Å. Data processing was performed by *HKL-2000* [24]. The structure of TlProR was determined by the molecular replacement method with PHASER [25] in CCP4 suite [26], for which the crystal structure of *Trypanosoma cruzi* proline racemase (PDB code, 1W61) was used as a search model. Further model building was performed manually with COOT [27], and crystallographic refinement with CNS [28] and PHENIX [29]. Detailed data collection and processing statistics are shown in Table 1.

2.3. Spectrophotometric enzyme assay

An L-proline oxidation assay was performed as follows. The reaction mixture contained 0.05 mM 2,6-dichloroindophenol (Cl₂I_{nd}) and purified L-ProDH (20 μg) in 50 mM Tris-HCl buffer (pH 8.0). The L-proline oxidation reaction was initiated by the addition of 1 mM TlProR (100 μL) or 20 mM Tris-HCl buffer (pH 8.0) containing 150 mM NaCl (100 μL) with a final reaction volume of 1 mL, and then the absorbance at 600 nm was measured at 50 °C using a Shimadzu UV-1800 spectrophotometer (Shimadzu GLC Ltd., Tokyo, Japan).

Racemase/epimerase activity of TlProR toward L-proline, T4LHyp, or T3LHyp was assayed at 50 °C by monitoring the reduction rate of an artificial electron acceptor in the coupling system with dehydrogenase for proline or hydroxyproline as described previously [19]. To measure the activity toward L-proline,

Table 1
Data collection and refinement statistics. Values in parentheses are for the highest resolution shell.

Data collection	
Space group	<i>P</i> 6 ₃ 22
<i>a</i> , <i>b</i> , <i>c</i> (Å)	125.38, 125.38, 140.63
Wavelength (Å)	1.00000
Resolution range (Å)	50.0–2.70 (2.75–2.70)
<i>R</i> _{merge}	0.180 (1.941)
<i>R</i> _{meas}	0.185 (1.993)
CC _{1/2} high resolution shell	0.734
<i>I</i> / <i>σ</i> (<i>I</i>)	25.4 (2.0)
Completeness (%)	100.0 (100.0)
Redundancy	20.1 (19.7)
Refinement	
Resolution (Å)	50.0–2.7
No. reflections	18,509
<i>R</i> / <i>R</i> _{free}	0.245/0.296
No. atoms	
Protein	2562
Ligand (proline)	8
Water	29
<i>B</i> -factors (Å ²)	
Protein	58.2
Ligand (proline)	58.8
Water	47.6
R.m.s. deviations	
Bond lengths (Å)	0.009
Bond angles (°)	1.0

10 mM L-proline was incubated with 0.05 mM Cl2Ind, purified D-ProDH (20 µg), and 50 nM TIPProR in 1 mL of 50 mM Tris-HCl buffer (pH 8.0). To measure the activity toward T4LHyp, 10 mM T4LHyp was incubated with 0.25 mM p-iodonitrotetrazolium violet, 0.06 mM phenazine methosulfate, purified D-HypDH (20 µg), and 50 nM TIPProR in 1 mL of 50 mM Tris-HCl buffer (pH 8.0). To measure the activity toward T3LHyp, 10 mM T3LHyp was incubated with 0.05 mM Cl2Ind, purified D-ProDH (20 µg), and 250 nM TIPProR in 1 mL of 50 mM Tris-HCl buffer (pH 8.0).

2.4. Amino acid sequence alignment

Amino acid sequences of TIPProR and its homologs were analyzed using the Clustal Omega [30] and ESPript 3.0 [31].

3. Results and discussion

3.1. Crystal structure of TIPProR

In order to elucidate the substrate recognition mechanism of TIPProR, we attempted to determine the crystal structure of TIPProR. TIPProR was expressed in *E. coli* cells, purified using (His)₆-tag affinity chromatography and size-exclusion chromatography. We obtained the TIPProR crystals belonging to the space group *P*6₃22. The crystal structure of TIPProR was determined using the molecular replacement method using the crystal structure of *T. cruzi* proline racemase (PDB code, 1W61) as a search model and subsequently refined to 2.7 Å resolution against the data set from a crystal of TIPProR (Table 1). The crystallographic asymmetric unit contains one TIPProR molecule, corresponding to a Matthews coefficient of 4.2 Å³Da⁻¹ and an estimated solvent content of 70.6%. The subunit forms the α/β fold comprised of four α-helices and three antiparallel β-sheets formed by 19 β-strands (Fig. 1A). To the best of our knowledge, this is the first structure of a bifunctional ProR/HypE from archaea. Similar to other proline racemase superfamily proteins [1,32], TIPProR forms a symmetric homodimer. The C-terminal β19 strand contributes to dimer formation by forming an intermolecular antiparallel β-sheet (Fig. 1A), and the gel-filtration analysis indicated that TIPProR exists as a dimer with a calculated MW of 76 kDa in solution (Fig. 1B). Structural comparison between TIPProR and other ProR superfamily proteins; *T. cruzi* ProR (PDB code, 1W61) and *Pseudomonas protegens* HypE (PDB code, 4J9X) [32] shows the r.m.s. differences of 1.4–1.7 Å, indicating that the structure of TIPProR is similar to those of other ProR superfamily proteins (Fig. 1C).

The dimer interface of TIPProR covers 1929.1 Å² (14% of the total surface area of one subunit) and is more extensive than those of *T. cruzi* ProR (1468.3 Å², 10% of the total surface area of one subunit) and *P. protegens* HypE (1161.9 Å², 9% of the total surface area of one subunit). The broad dimer interface area may contribute to the extreme thermostability of TIPProR.

3.2. A proline molecule is tightly bound to recombinant TIPProR

Surprisingly, clear electron density was observed in the active site in the center of the TIPProR molecule, although no substrate was added during purification and crystallization (Fig. 2A). We assumed that an L-proline derived from *E. coli* cells is bound to the active site of TIPProR in the crystal. The proline molecule fitted well into the electron density map and was completely enclosed by TIPProR, suggesting that TIPProR forms a substrate-binding closed conformation (Fig. 2A and B). The Cα atom of proline is in close contact with the SH groups of catalytic cysteine residues (Cys88 and Cys251). To confirm that the proline molecule exists in purified TIPProR, we performed the L-proline oxidation assay using purified L-ProDH and an artificial

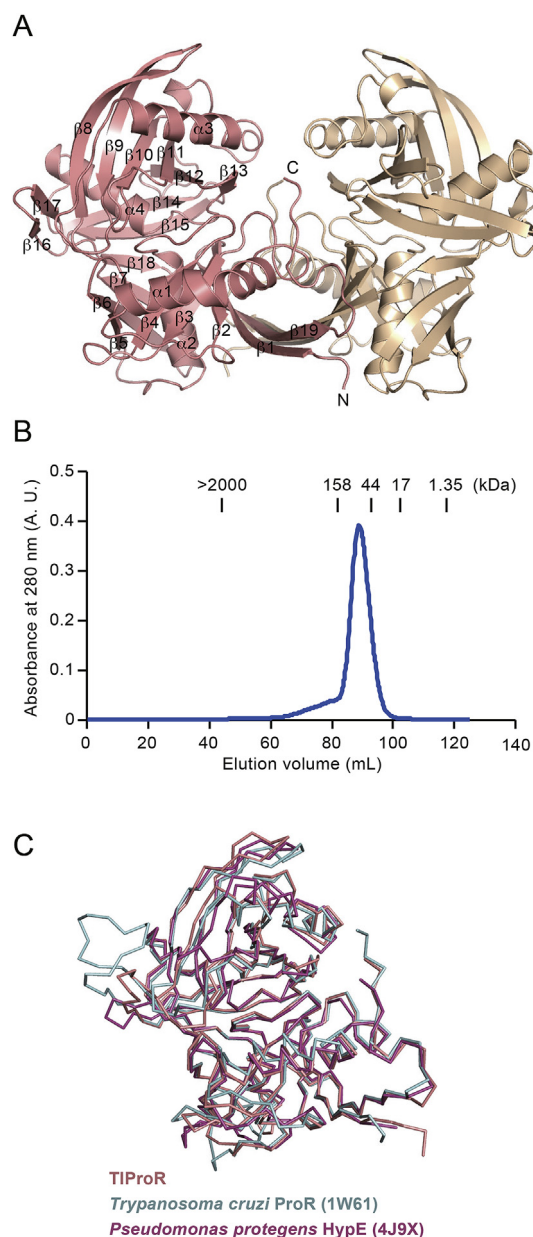


Fig. 1. Crystal structure of TIPProR. (A) Overall structure of a TIPProR dimer with one subunit in pink and another subunit in light brown. (B) Gel-filtration elution profile of TIPProR showing that TIPProR exists as a dimer in solution. The void volume (>2000 kDa) and molecular weight markers are indicated. (C) Superposition of TIPProR (pink), *T. cruzi* ProR (cyan) and *P. protegens* HypE (magenta). (For interpretation of the references to colour in this figure legend, the reader is referred to the Web version of this article.)

electron acceptor, Cl2Ind. L-ProDH catalyzes the oxidation of L-proline to Δ¹-pyrroline-5-carboxylate with reduction of Cl2Ind [21]. The assay is based on spectrophotometrically monitoring the decrease of Cl2Ind that absorbs at 600 nm. In the assay, purified L-ProDH and TIPProR are incubated with Cl2Ind, and oxidation of L-proline bound to TIPProR by L-ProDH will lead to reduction of Cl2Ind i.e. decrease in the absorbance at 600 nm. As shown in Fig. 2C, in the presence of TIPProR, absorbance at 600 nm was efficiently decreased in a time-dependent manner as compared with the negative control without TIPProR (Fig. 2C). These results indicated that the proline molecule derived from *E. coli* cells is tightly bound to the purified TIPProR during purification and crystallization, and that TIPProR co-crystallized with the proline molecule.

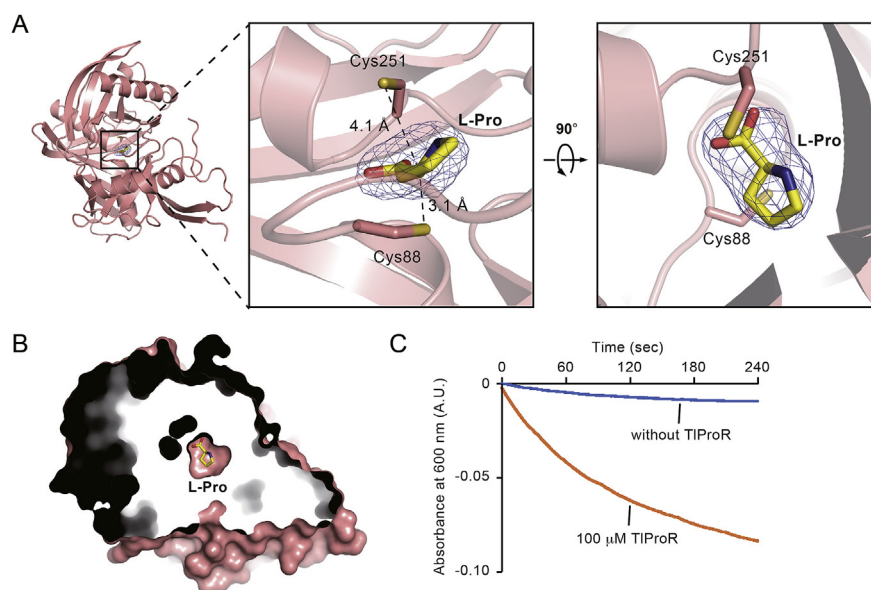


Fig. 2. The proline molecule bound to TIPProR. (A) Electron density map of the bound proline molecule. The simulated annealing F_0-F_c difference Fourier map was calculated by omitting the proline molecule, and is shown with blue meshes countered at 3.0σ . Distances from the $C\alpha$ atom of the bound proline to the sulfur atoms of Cys88 and Cys251 are indicated. (B) Cutaway representation of TIPProR at the level of the active site. The bound proline molecule is shown as a stick model. (C) 100 μ M TIPProR or buffer (indicated as “without TIPProR”) was mixed with 0.05 mM Cl2Ind and purified L-ProDH (20 μ g), and then the absorbance at 600 nm was monitored at 50 °C for 240 s. (For interpretation of the references to colour in this figure legend, the reader is referred to the Web version of this article.)

3.3. Substrate recognition mechanism of TIPProR

The bound proline molecule is entirely buried in the mostly hydrophobic active site of TIPProR, as shown in Fig. 3A. In the active site, the side chain carboxylic oxygen atom of Asp247 is within the distance that allows the formation of hydrogen bonds with the pyrrolidine nitrogen atom of the bound proline, and the imidazolyl nitrogen atom of His90 and the hydroxyl oxygen atom of Thr253 are within the distance that allows the formation of hydrogen bonds with the carboxylate group of the bound proline. The hydrophobic pyrrolidine ring is in contact with hydrophobic side chains of Phe62, Leu85, Tyr171, Leu221, and Trp241 in the active site (Fig. 3A). These interactions of TIPProR and the substrate are partially similar to those of ProR superfamily proteins (e.g. *T. cruzi* ProR and *P. protegens* HypE; Fig. 3B and C). Structural comparison among these enzymes showed that Trp241 in TIPProR is substituted to Phe290 in *T. cruzi* ProR and that Leu221 and Trp241 in TIPProR are substituted to His208 and Cys226 in *P. protegens* HypE, respectively. The side chain of Phe290 in *T. cruzi* ProR is in contact with the hydrophobic pyrrole ring of the bound inhibitor pyrrole-2-carboxylic acid (PYC) (Fig. 3B). The side chains of His208 and

Cys226 in *P. protegens* HypE are close to the hydroxyl oxygen atom of the bound T4LHyp (Fig. 3C). These observations suggested that these residues are responsible for the substrate specificity. Actually, a previous study showed that L221H and W241F mutations in TIPProR resulted in a shift in substrate specificity toward proline and 4-hydroxyproline, respectively [19]. In the TIPProR structure, the indole nitrogen atom of Trp241 is relatively close to the C-4 atom of the bound proline, suggesting that Trp241 makes a hydrogen bond with the hydroxyl oxygen atom of 4-hydroxyproline and thus contributes to the substrate specificity toward 4-hydroxyproline (Fig. 3A). On the other hand, the hydroxyl oxygen atom of Tyr171 in TIPProR is relatively close to the C-3 atom of the bound proline, suggesting that Tyr171 contributes to the substrate specificity toward 3-hydroxyproline (Fig. 3A).

3.4. Mutational analyses of the substrate binding site of TIPProR

To further investigate the roles of Tyr171 and Trp241 in the substrate specificity of TIPProR, we introduced mutations to Tyr171 and Trp241, and measured the activities for L-proline, T4LHyp and T3LHyp (Fig. 4A and B). The W241F mutation slightly increased the

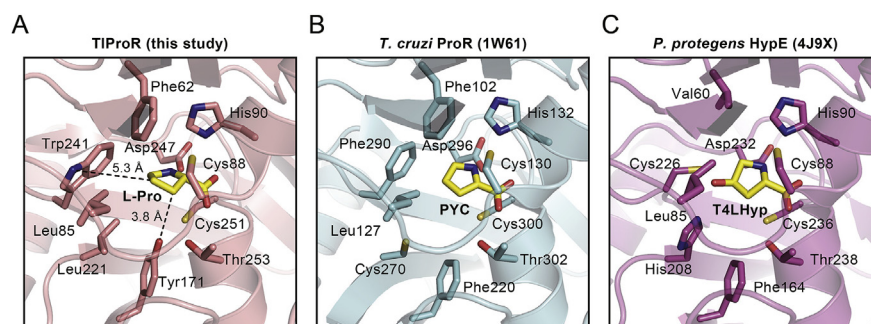


Fig. 3. Structural comparison. Close-up view of the substrate binding sites of (A) TIPProR, (B) *T. cruzi* ProR and (C) *P. protegens* HypE. Distances between the indole nitrogen atom of Trp241 in TIPProR and the C-4 atom of the bound proline and between the hydroxyl oxygen atom of Tyr171 in TIPProR and the C-3 atom of the bound proline are indicated.

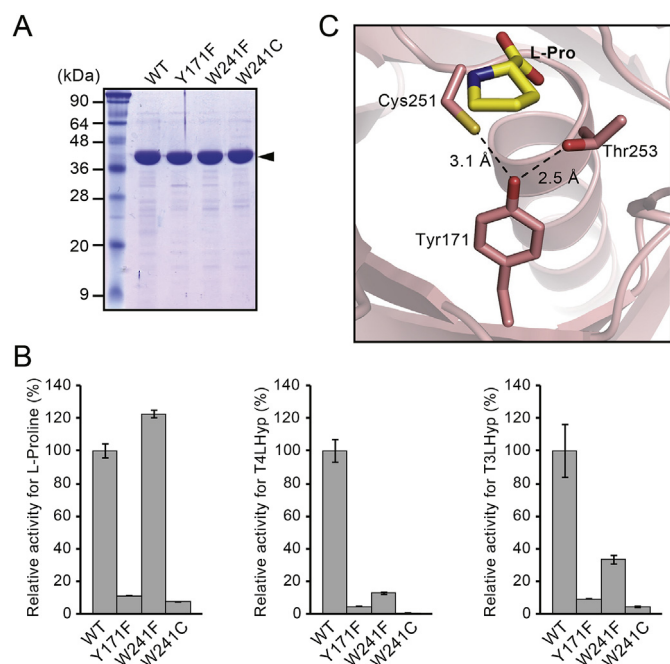


Fig. 4. Site-directed mutagenesis of Tyr171 and Trp241 in TIPrOR. (A) Purified TIPrOR mutants were analyzed by SDS-PAGE followed by CBB staining. The arrowhead indicates purified TIPrOR. (B) Measurement of racemase/epimerase activities of TIPrOR mutants toward L-proline (left panel), T4LHyp (center panel), and T3LHyp (right panel) by spectrophotometric enzyme assay (see details in Materials and methods). The activity of wild-type TIPrOR was set to 100%. Values are mean \pm SEM ($n = 3$). (C) Close view of Tyr171 in TIPrOR. Broken lines designate possible hydrogen bonds.

racemase activity with L-proline and significantly decreased the epimerase activities with T4LHyp and T3LHyp (Fig. 4B), consistent with the previous mutational analyses [19]. On the other hand, the W241C mutation abolished both the racemase and epimerase activities, suggesting that the bulky aromatic residue at the Trp241 position in TIPrOR is essential for both the racemase and epimerase activities of TIPrOR. However, *P. protegens* HypE has a conserved cysteine residue (Cys226) at the Trp241 position in TIPrOR (Fig. 3C and Fig. S1). A proline residue next to Cys226 in *P. protegens* HypE is also conserved in the HypE subfamily and, therefore, might contribute to the proper formation of the substrate binding site of *P. protegens* HypE. Unexpectedly, the Y171F mutation also abolished both the racemase and epimerase activities (Fig. 4B), although Tyr171 in TIPrOR is substituted to phenylalanine in the ProR subfamily and HypE subfamily (Fig. S1). The hydroxyl oxygen atom of Tyr171 is within the distance that allows the formation of hydrogen bonds with the hydroxyl oxygen atom of Thr253 and the sulfur atom of catalytic Cys251 (Fig. 4C). Given that Tyr171 is conserved in the bifunctional ProR/HypE subfamily from hyperthermophilic archaea but not in the ProR subfamily and HypE subfamily (Fig. S1), Tyr171 in TIPrOR may contribute to the thermostability, rather than substrate specificity, by the formation of hydrogen bonds with catalytic residues. However, Tyr171 is also conserved in the T3LHypD subfamily (Fig. S1), implying that the tyrosine residue in T3LHypD has a possible role not only in thermostability, but also in substrate recognition for T3LHyp.

In this study, we solved the crystal structure of TIPrOR in a complex with proline molecule at 2.7 Å resolution and proposed that Trp241 and Tyr171 are responsible for substrate specificity and thermostability, respectively. Further structural studies for TIPrOR in complex with 4-hydroxyproline or 3-hydroxyproline will shed light on understanding the precise molecular mechanism of the unique substrate specificity.

Accession number

The coordinates and structural factors of TIPrOR have been deposited under the Protein Data Bank accession code: 6J7C.

Conflicts of interest

The authors declare no conflicts of interest associated with this manuscript.

Acknowledgments

We would like to thank the staff at beamline BL38B1 of SPring-8, Japan for data collection support. This work was supported by JSPS KAKENHI Grant 16K07297 (to S.W.) and the Sumitomo Foundation (Basic Science Research Projects) (to S.W.).

Appendix A. Supplementary data

Supplementary data to this article can be found online at <https://doi.org/10.1016/j.bbrc.2019.01.141>.

References

1. A. Buschiazio, M. Goytia, F. Schaeffer, W. Degraeve, W. Shepard, C. Gregoire, N. Chamond, A. Cosson, A. Berneman, N. Coatnoan, P.M. Alzari, P. Minoprio, Crystal structure, catalytic mechanism, and mitogenic properties of Trypanosoma cruzi proline racemase, Proc. Natl. Acad. Sci. U.S.A. 103 (2006) 1705–1710.
2. M. Stenta, M. Calvaresi, P. Altoe, D. Spinelli, M. Garavelli, A. Bottoni, The catalytic activity of proline racemase: a quantum mechanical/molecular mechanical study, J. Phys. Chem. B 112 (2008) 1057–1059.
3. A. Rubinstein, D.T. Major, Catalyzing racemizations in the absence of a cofactor: the reaction mechanism in proline racemase, J. Am. Chem. Soc. 131 (2009) 8513–8521.
4. S. Jackson, M. Calos, A. Myers, W.T. Self, Analysis of proline reduction in the nosocomial pathogen Clostridium difficile, J. Bacteriol. 188 (2006) 8487–8495.
5. L. Bouillaut, W.T. Self, A.L. Sonenshein, Proline-dependent regulation of Clostridium difficile Stickland metabolism, J. Bacteriol. 195 (2013) 844–854.
6. B. Reina-San-Martin, W. Degraeve, C. Rougeot, A. Cosson, N. Chamond, A. Cordeiro-Da-Silva, M. Arala-Chaves, A. Coutinho, P. Minoprio, A B-cell mitogen from a pathogenic trypanosome is a eukaryotic proline racemase, Nat. Med. 6 (2000) 890–897.
7. N. Chamond, C. Gregoire, N. Coatnoan, C. Rougeot, L.H. Freitas-Junior, J.F. da Silva, W.M. Degraeve, P. Minoprio, Biochemical characterization of proline racemases from the human protozoan parasite Trypanosoma cruzi and definition of putative protein signatures, J. Biol. Chem. 278 (2003) 15484–15494.
8. N. Chamond, A. Cosson, N. Coatnoan, P. Minoprio, Proline racemases are conserved mitogens: characterization of a Trypanosoma vivax proline racemase, Mol. Biochem. Parasitol. 165 (2009) 170–179.
9. N. Chamond, M. Goytia, N. Coatnoan, J.C. Barale, A. Cosson, W.M. Degraeve, P. Minoprio, Trypanosoma cruzi proline racemases are involved in parasite differentiation and infectivity, Mol. Microbiol. 58 (2005) 46–60.
10. N. Coatnoan, A. Berneman, N. Chamond, P. Minoprio, Proline racemases: insights into Trypanosoma cruzi peptides containing D-proline, Mem. Inst. Oswaldo Cruz 104 (Suppl 1) (2009) 295–300.
11. E. Adams, L. Frank, Metabolism of proline and the hydroxyprolines, Annu. Rev. Biochem. 49 (1980) 1005–1061.
12. R. Hara, N. Uchiyumi, N. Okamoto, K. Kino, Regio- and stereoselective oxygenation of proline derivatives by using microbial 2-oxoglutarate-dependent dioxygenases, Biosci. Biotechnol. Biochem. 78 (2014) 1384–1388.
13. S. Watanabe, M. Yamada, I. Ohtsu, K. Makino, alpha-ketoglutaric semialdehyde dehydrogenase isozymes involved in metabolic pathways of D-glucarate, D-galactarate, and hydroxy-L-proline. Molecular and metabolic convergent evolution, J. Biol. Chem. 282 (2007) 6685–6695.
14. S. Watanabe, D. Morimoto, F. Fukumori, H. Shinomiya, H. Nishiwaki, M. Kawano-Kawada, Y. Sasai, Y. Tozawa, Y. Watanabe, Identification and characterization of D-hydroxyproline dehydrogenase and Delta1-pyrroline-4-hydroxy-2-carboxylate deaminase involved in novel L-hydroxyproline metabolism of bacteria: metabolic convergent evolution, J. Biol. Chem. 287 (2012) 32674–32688.
15. W.F. Visser, N.M. Verhoeven-Duif, T.J. de Koning, Identification of a human trans-3-hydroxy-L-proline dehydratase, the first characterized member of a novel family of proline racemase-like enzymes, J. Biol. Chem. 287 (2012) 21654–21662.
16. S. Watanabe, Y. Tanimoto, S. Yamauchi, Y. Tozawa, S. Sawayama, Y. Watanabe, Identification and characterization of trans-3-hydroxy-L-proline dehydratase

- and Delta(1)-pyrroline-2-carboxylate reductase involved in trans-3-hydroxy-L-proline metabolism of bacteria, *FEBS Open Bio* 4 (2014) 240–250.
- [17] S. Watanabe, Y. Tozawa, Y. Watanabe, Ornithine cyclodeaminase/mu-crystallin homolog from the hyperthermophilic archaeon *Thermococcus litoralis* functions as a novel Delta(1)-pyrroline-2-carboxylate reductase involved in putative trans-3-hydroxy-L-proline metabolism, *FEBS Open Bio* 4 (2014) 617–626.
- [18] M. Goytia, N. Chamond, A. Cosson, N. Coatnoan, D. Hermant, A. Berneman, P. Minoprio, Molecular and structural discrimination of proline racemase and hydroxyproline-2-epimerase from nosocomial and bacterial pathogens, *PLoS One* 2 (2007) e885.
- [19] S. Watanabe, Y. Tanimoto, H. Nishiwaki, Y. Watanabe, Identification and characterization of bifunctional proline racemase/hydroxyproline epimerase from archaea: discrimination of substrates and molecular evolution, *PLoS One* 10 (2015) e0120349.
- [20] H. Sakuraba, T. Satomura, R. Kawakami, K. Kim, Y. Hara, K. Yoneda, T. Ohshima, Crystal structure of novel dye-linked L-proline dehydrogenase from hyperthermophilic archaeon *Aeropyrum pernix*, *J. Biol. Chem.* 287 (2012) 20070–20080.
- [21] T. Satomura, Y. Hara, S. Suye, H. Sakuraba, T. Ohshima, Gene expression and characterization of a third type of dye-linked L-proline dehydrogenase from the aerobic hyperthermophilic archaeon, *Aeropyrum pernix*, *Biosci. Biotechnol. Biochem.* 76 (2012) 589–593.
- [22] T. Satomura, R. Kawakami, H. Sakuraba, T. Ohshima, Dye-linked D-proline dehydrogenase from hyperthermophilic archaeon *Pyrobaculum islandicum* is a novel FAD-dependent amino acid dehydrogenase, *J. Biol. Chem.* 277 (2002) 12861–12867.
- [23] S. Watanabe, Y. Hiraoka, S. Endo, Y. Tanimoto, Y. Tozawa, Y. Watanabe, An enzymatic method to estimate the content of L-hydroxyproline, *J. Biotechnol.* 199 (2015) 9–16.
- [24] Z. Otwinowski, W. Minor, Processing of X-ray diffraction data collected in oscillation mode, *Methods Enzymol.* 276 (1997) 307–326.
- [25] A.J. McCoy, R.W. Grosse-Kunstleve, P.D. Adams, M.D. Winn, L.C. Storoni, R.J. Read, Phaser crystallographic software, *J. Appl. Crystallogr.* 40 (2007) 658–674.
- [26] M.D. Winn, C.C. Ballard, K.D. Cowtan, E.J. Dodson, P. Emsley, P.R. Evans, R.M. Keegan, E.B. Krissinel, A.G. Leslie, A. McCoy, S.J. McNicholas, G.N. Murshudov, N.S. Pannu, E.A. Potterton, H.R. Powell, R.J. Read, A. Vagin, K.S. Wilson, Overview of the CCP4 suite and current developments, *Acta Crystallogr. D. Biol. Crystallogr.* 67 (2011) 235–242.
- [27] P. Emsley, B. Lohkamp, W.G. Scott, K. Cowtan, Features and development of coot, *Acta Crystallogr. D. Biol. Crystallogr.* 66 (2010) 486–501.
- [28] A.T. Brunger, P.D. Adams, G.M. Clore, W.L. DeLano, P. Gros, R.W. Grosse-Kunstleve, J.S. Jiang, J. Kuszewski, M. Nilges, N.S. Pannu, R.J. Read, L.M. Rice, T. Simonson, G.L. Warren, Crystallography & NMR system: a new software suite for macromolecular structure determination, *Acta Crystallogr. D. Biol. Crystallogr.* 54 (1998) 905–921.
- [29] P.D. Adams, P.V. Afonine, G. Bunkoczi, V.B. Chen, I.W. Davis, N. Echols, J.J. Headd, L.W. Hung, G.J. Kapral, R.W. Grosse-Kunstleve, A.J. McCoy, N.W. Moriarty, R. Oeffner, R.J. Read, D.C. Richardson, J.S. Richardson, T.C. Terwilliger, P.H. Zwart, PHENIX: a comprehensive Python-based system for macromolecular structure solution, *Acta Crystallogr. D. Biol. Crystallogr.* 66 (2010) 213–221.
- [30] F. Sievers, A. Wilm, D. Dineen, T.J. Gibson, K. Karplus, W. Li, R. Lopez, H. McWilliam, M. Remmert, J. Soding, J.D. Thompson, D.G. Higgins, Fast, scalable generation of high-quality protein multiple sequence alignments using Clustal Omega, *Mol. Syst. Biol.* 7 (2011) 539.
- [31] X. Robert, P. Gouet, Deciphering key features in protein structures with the new ENDscript server, *Nucleic Acids Res.* 42 (2014) W320–W324.
- [32] S. Zhao, A. Sakai, X. Zhang, M.W. Vetting, R. Kumar, B. Hillerich, B. San Francisco, J. Solbiati, A. Steves, S. Brown, E. Akiva, A. Barber, R.D. Seidel, P.C. Babbitt, S.C. Almo, J.A. Gerlt, M.P. Jacobson, Prediction and characterization of enzymatic activities guided by sequence similarity and genome neighborhood networks, *Elife* 3 (2014).